

Article

# Study of the Cone-Shaped Drogue for a Deep-Towed Multi-Channel Seismic Survey System Based on Data-Driven Simulations

Xiangqian Zhu <sup>1,2,\*</sup>, Mingqi Sun <sup>1,2</sup>, Tianhao He <sup>1</sup>, Kaiben Yu <sup>3</sup>, Le Zong <sup>3</sup> and Jin-Hwan Choi <sup>4</sup>

- <sup>1</sup> Key Laboratory of High-Efficiency and Clean Mechanical Manufacture, School of Mechanical Engineering, Shandong University, Jinan 250012, China; 202034365@mail.sdu.edu.cn (M.S.); 201700162151@mail.sdu.edu.cn (T.H.)
- <sup>2</sup> National Demonstration Center for Experimental Mechanical Engineering Education at Shandong University, Jinan 250012, China
- <sup>3</sup> National Deep Sea Center, Qingdao 266237, China; yukb@ndsc.org.cn (K.Y.); zongl@ndsc.org.cn (L.Z.)
- <sup>4</sup> Department of Mechanical Engineering, Kyunghee University, Yongin 17104, Korea; jhchoi@khu.ac.kr
- \* Correspondence: xqzhu@sdu.edu.cn

**Abstract:** A drogue is used to stabilise and straighten seismic arrays so that seismic waves can be well-received. To embed the effect of a cone-shaped drogue into the numerical modelling of the deep-towed seismic survey system, one surrogate model that maps the relationship between the hydrodynamic characteristics of the drogue and towing conditions was obtained based on data-driven simulations. The sample data were obtained by co-simulation of the commercial software RecurDyn and Particleworks, and the modelling parameters were verified by physical experiments. According to the Morison formula, the rotational angle, angular velocity, angular acceleration, towing speed, and towing acceleration of the drogue were selected as the design variables and drag forces and aligning torque were selected as the research objectives. The sample data of more than 8500 sets were obtained from virtual manoeuvres. Subsequently, both polynomial and neural network regression algorithms were used to study these data. Finally, analysis results show that the surrogate model obtained by machine learning has good performance in predicting research objectives. The results also reveal that the neural network regression algorithm is superior to the polynomial regression algorithm, its largest error of mean square is less than  $0.8 (N^2/N^2 \text{ mm}^2)$ , and its R-squared is close to 1.

**Keywords:** cone-shaped drogue; hydrodynamic force; virtual simulation; machine learning



**Citation:** Zhu, X.; Sun, M.; He, T.; Yu, K.; Zong, L.; Choi, J.-H. Study of the Cone-Shaped Drogue for a Deep-Towed Multi-Channel Seismic Survey System Based on Data-Driven Simulations. *J. Mar. Sci. Eng.* **2021**, *9*, 1367. <https://doi.org/10.3390/jmse9121367>

Academic Editors: Yigit Kemal Demirel and Soonseok Song

Received: 11 October 2021  
Accepted: 23 November 2021  
Published: 2 December 2021

**Publisher's Note:** MDPI stays neutral with regard to jurisdictional claims in published maps and institutional affiliations.



**Copyright:** © 2021 by the authors. Licensee MDPI, Basel, Switzerland. This article is an open access article distributed under the terms and conditions of the Creative Commons Attribution (CC BY) license (<https://creativecommons.org/licenses/by/4.0/>).

## 1. Introduction

A deep-towed multi-channel seismic survey system, consisting of mothership, towing cable, towed vehicle, seismic array, and drogue, is used for high-resolution surveys of the submarine stratum, as shown in Figure 1 [1,2]. The towed seismic array is used to collect seismic waves reflected from different strata. The heavy pitching motions of the towed vehicle disturb the towed seismic array and ultimately affect the measurement accuracy. Therefore, reducing the swing of the seismic array and maintaining its straight shape is key to improving the exploration resolution. The drogue installed at the tail of the seismic array can provide backward drag resistance, which can effectively reduce the swing of the seismic array. Sengupta et al. [3] examined the performance of a conical ribbon drogue parachute in the wake of a subscale Orion command module. The drogue can provide command module stabilisation and deceleration prior to the main parachute deploy. The disk-gap-band (DGB)-type supersonic parachute is traditionally adopted for future manned planetary exploration, and the parachute exhibits the open areas. The flow of air from the open areas reduces the force generated during parachute inflation [4]. Since the cone-shaped structure has superior alignability and returnability, a cone-shaped drogue with both circular sections opened was therefore chosen for this study. The deep-towed multi-channel seismic survey system is mainly composed of slender cables that are

thousands of metres, and much computation time is needed when the whole system is analysed using computational fluid dynamics (CFD). The hydrodynamics of slender cables can be calculated simply by using the Morison formula, which is inapplicable to cone-shaped drogues [5–7]. Therefore, one surrogate model that maps the relationship between the hydrodynamic characteristics of the cone-shaped drogue and towing conditions was obtained in advance by the machine-learning technique herein described, and this surrogate model will be embedded into the numerical modelling of the deep-towed multi-channel seismic survey system for later towing-operation optimization and components design.

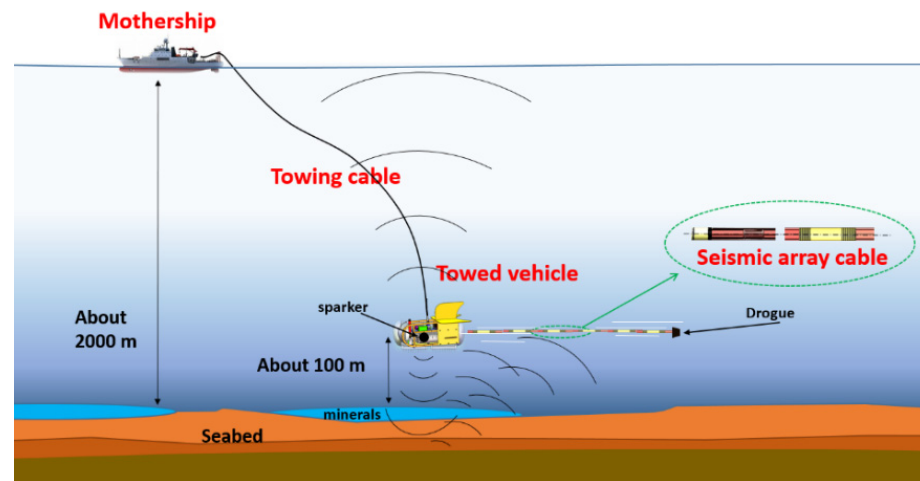


**Figure 1.** Deep-towed multi-channel seismic survey system.

Building a data library is one critical process in machine learning. To build this data library, hydrodynamic characteristics of the cone-shaped drogue can be analysed by traditional CFD methods, such as the finite volume method or the finite difference method [8]. However, the drogue moves freely during towing conditions and the moving boundary condition severely limits the efficiency of the solution provided by traditional CFD methods [9]. Moving Particle Semi-implicit (MPS) is one kind of mesh-free particle method, developed by Koshizuka [10,11], and the fluid is stable at the wall boundary [12]. The commercial software Particleworks has been used to analyse oil lubrication of the gearbox and interaction between ocean wave and ship [13,14]. The computation speed is faster with the parallel computing. Therefore, the data library was generated by the co-simulation of RecurDyn and Particleworks herein [15]. To ensure the accuracy of the simulation results, physical experiments were conducted using circulating water tanks in the National Deep Sea Center. Both the particle size and integration step were tuned according to the results provided by the experiments. At the same time, a machine-learning technique is a data-driven information-processing framework that can extract potential information from a large amount of data, build models, and overcome the limitations of traditional research methods [16]. At present, research on the intersection of fluid mechanics and machine learning mainly focuses on the reconstruction of the flow field and the mapping of characteristic quantities such as force coefficients [17,18]. Aiming at turbulent flow field reconstruction, Milano et al. [19] realised the reconstruction and prediction of the near-wall flow field through the wall pressure and shear-stress two-wall information. Fukami et al. [20] used the convolutional neural network and the hybrid down-sampled skip-connection/multi-scale models to perform a super-resolution analysis of grossly under-resolved turbulent flow field data, to reconstruct the high-resolution flow field. To map the force coefficients and other characteristic quantities, Lin et al. [21] established a neural network that can calculate the hydrodynamic coefficient of the Morison formula under different Reynolds numbers, KC numbers, and roughness values. The M5 model tree and nonlinear regression method were used to solve the hydrodynamic coefficients on vertical piles in regular waves [22]. Several years later, a hybrid model of

the M5 model tree and a genetic algorithm was proposed [23]. The advantages of the two algorithms were used to process the wave-load data of the pile group, and the relations among the coefficients of the pile group, KC number, pile-group arrangement, and relative pile distance were derived. Srinivasan et al. [24] used the multilayer perceptron and the long short-term memory (LSTM) to predict temporally evolving turbulent flows. The LSTM led to excellent predictions of turbulence statistics and the dynamical behaviour of the system networks. Theodoropoulos et al. [25] researched the development of deep-learning models that can be utilised to predict the propulsion power of a vessel. They also evaluated feed-forward neural networks and recurrent neural networks. Predictions provided by these models were compared with values measured onboard. Machine learning offers a wealth of techniques to extract information from data that can be translated into knowledge about the underlying fluid mechanics. Therefore, it is feasible to establish the surrogate model using the machine-learning method in this study.

The relationship between the hydrodynamic characteristics of the cone-shaped drogue and towing conditions can be studied using data-driven simulations. Firstly, according to the Morison formula, the rotational angle, angular velocity, angular acceleration, towing speed, and towing acceleration were selected as design variables. The drag forces and aligning torque were selected as the research objectives. According to the motion characteristics of the towed vehicle and the cone-shaped drogue in the actual sea trial, a reasonable range of each design variable, that covered all towing conditions, was set. Sample data was obtained by co-simulation of the commercial softwares RecurDyn and Particleworks. The modelling parameters were verified by physical experiments. Geometric objects and kinematic pairs were modelled in RecurDyn, and the liquid flow was simulated by particles generated in Particleworks. By adjusting the towing speed and rotational angle, nine series of simulation data were collected and more than 8500 sets of data were obtained. After data cleaning, coordinate conversion, and low-pass filtering, the data library was established. Subsequently, both polynomial and neural network regression algorithms were used to study these data. The surrogate model was generated using 60% of the data, algorithm parameters were corrected using 20% of the data, and the remaining 20% of the data were used to test this surrogate model. Finally, analysis results show that the surrogate model obtained by machine learning had good performance in predicting research objectives. The results also reveal that the neural network regression algorithm is superior to the polynomial regression algorithm, its largest error of mean square is less than 0.8 ( $N^2/N^2 \cdot \text{mm}^2$ ), and its R-squared is close to 1. Section 2 describes the numerical model used in this study. Section 3 introduces the physical experiment. Section 4 completes the calibration of the simulation model and introduces the data library. Section 5 introduces the algorithms and results. Section 6 summarises the outcomes of the research.

## 2. Numerical Model

There is no established mathematical formula for calculating the hydrodynamics of a cone-shaped drogue model. However, the hydrodynamics of cylindrical marine structures with relatively small dimensions (ratio of characteristic size to wave wavelength less than 0.2) can be calculated using the Morison formula. Morison asserts that the forces acting on the structure are divided into two parts. One is the horizontal viscous resistance force  $f_D$ , which is caused by the horizontal velocity  $u_x$  of the motion of water particles, and the other is the inertial force  $f_I$ , which is caused by the horizontal acceleration  $\partial u_x / \partial t$  of the motion of water particles. The specific formula is given by Equation (3):

$$f_D = \frac{1}{2} C_D \rho A u_x |u_x|. \quad (1)$$

$$f_I = C_M \rho V \frac{\partial u_x}{\partial t}. \quad (2)$$

$$f = f_D + f_I = \frac{1}{2} C_D \rho A u_x |u_x| + C_M \rho V \frac{\partial u_x}{\partial t}. \quad (3)$$

where  $u_x$  is the horizontal velocity of the wave water point,  $\partial u_x / \partial t$  is the horizontal acceleration,  $A$  is the projected area of an object in the direction of movement,  $V$  is the drainage volume of the structure,  $\rho$  is the water density,  $C_D$  is the drag resistance coefficient (drag coefficient, velocity force coefficient), and  $C_M$  is the coefficient of inertia force (mass coefficient).

According to the Morison formula, the hydrodynamic forces of a cone-shaped drogue are closely related to its velocity and acceleration relative to the surrounding water, the projected area in the direction of movement, the volume of displacement, the density of water, the drag resistance coefficient, and the coefficient of inertia force. Since the density of water and the size of the cone-shaped drogue are constant and the drainage volume is small, the drag resistance coefficient and the coefficient of inertia force change with the motions and orientation of the drogue. The towing speed, acceleration, and rotational angle of the drogue were chosen as the design variables. Since the angle changes unevenly with time, the angular velocity and angular acceleration were also introduced as design variables. The coordinate system is shown in Figure 2. The design variables are the rotational angle, angular velocity, and angular acceleration in the Z direction, towing speed, and acceleration along the X direction. The cone-shaped drogue is symmetrical about its central axis, as shown in Figure 2. Thus, the research targets are the axial drag force in the X and Y directions, and the torque in the Z direction.

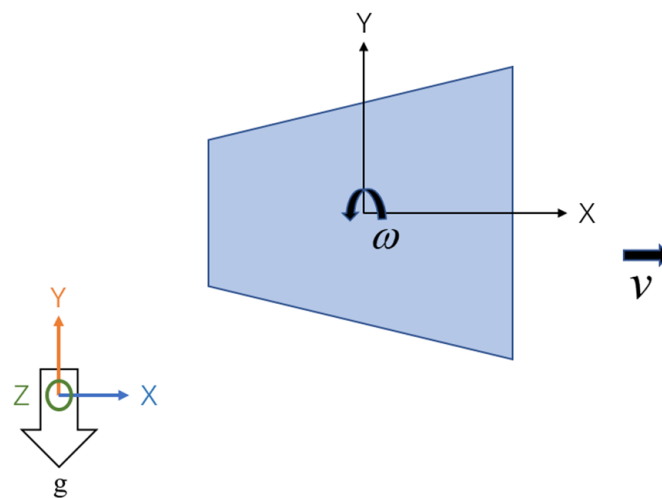


**Figure 2.** Coordinate system of cone-shaped drogue.

The sample data can be obtained by virtual simulations and physical experiments. Those obtained by physical experiments are highly reliable, but the experiments are time-consuming and costly. The efficiency of data acquisition by simulation is high, but its accuracy needs to be verified. Since a number of data is needed and the cost of physical experiments is high, the data library was created by virtual simulations. To improve the accuracy, experimental data was collected for the subsequent simulation calibration. A simulation model was constructed with the same experimental conditions, and parameters such as particle diameter and integration step were adjusted to make the simulation results close to the experimental data, so as to improve the reliability of the simulation analysis results.

### 3. Physical Experiment

The axial drag forces of one cone-shaped drogue were measured by using unidirectional tension sensor, and the measured axial drag forces helped to tune modelling parameters of the virtual simulation. The experimental facilities and efforts in improving the accuracy of experiments are introduced herein.

### 3.1. Circulating Water Tank Equipment

This experiment was carried out with the aid of a circulating water tank in the National Deep Sea Center. The circulating water tank is mainly composed of a flow rate controller, a fluid adjusting and stabilising system, and a working part, as shown in Figure 3. The working part is made of transparent glass, and both height and width of the cross-section are 400 mm. The range of the steady flow is from 0.1 m/s to 1.0 m/s. The water speed of the working part can be controlled by adjusting the frequency of the converter using the flow rate controller, as shown in Figure 4.

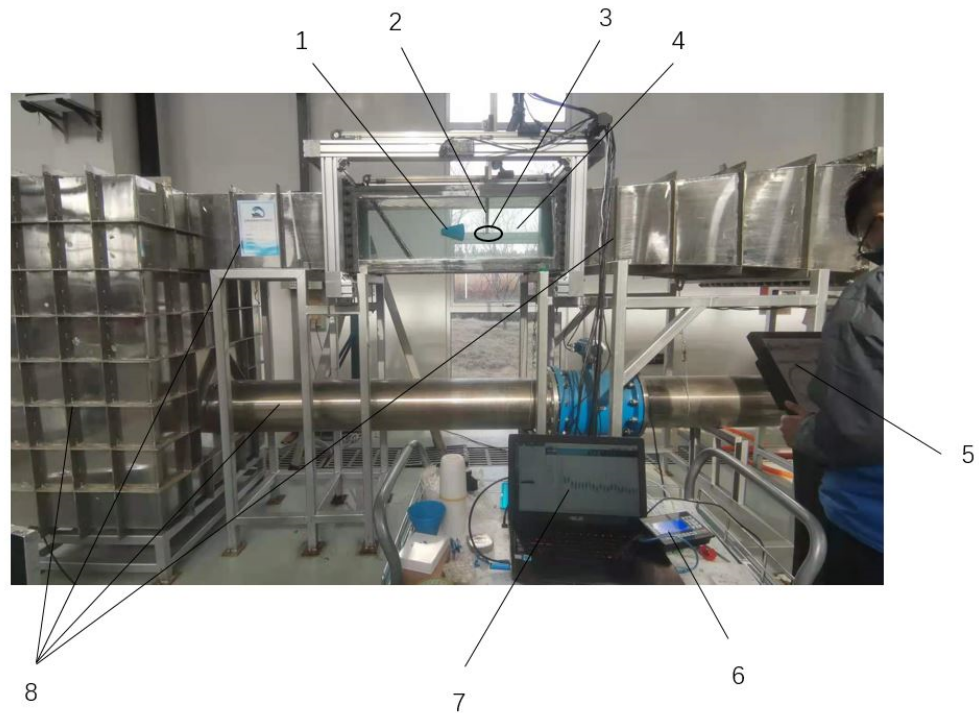


**Figure 3.** Circulating water tank and measuring system in physical experiment, 1: cone-shaped drogue; 2: airfoiled plate; 3: tension sensor; 4: working part; 5: flow rate controller; 6: drogue position controller; 7: load data indicator; 8: fluid adjusting and stabilising system.

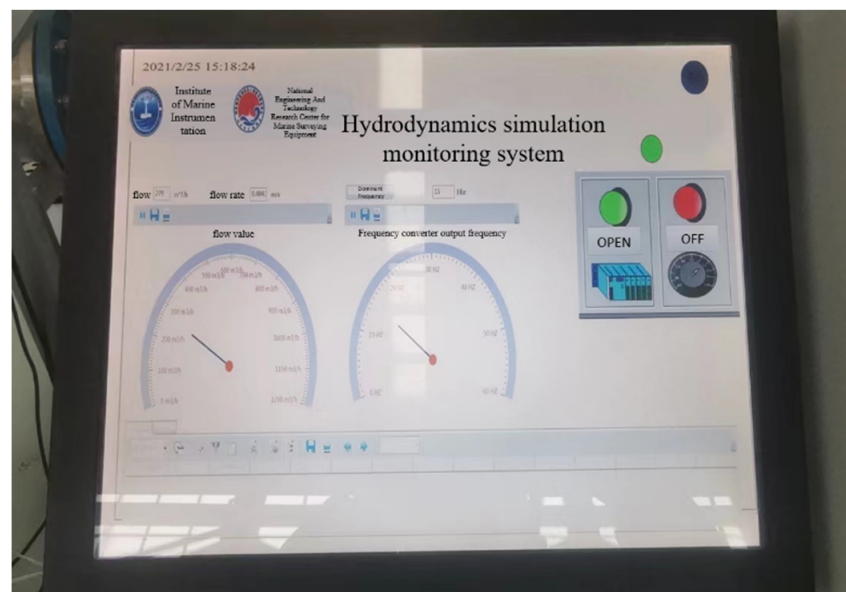


**Figure 4.** Interface of flow rate controller.

### 3.2. Data Collection

The cone-shaped drogue was tied to one end of the tension sensor by four nylon lines, and the other end of the sensor was connected to the bottom of the airfoiled plate through a threaded connection, as shown in Figure 5a. The NACA0021 airfoiled plate with a low Mach number and a high angle of attack was selected as the sensor mounting frame, to reduce the disturbance to the flow field. Figure 5b illustrates that the airfoiled plate had a slight influence on the flow field behind. The cone-shaped drogue was placed at the centre of the tank to prevent the drogue from touching the wall during the experiment.

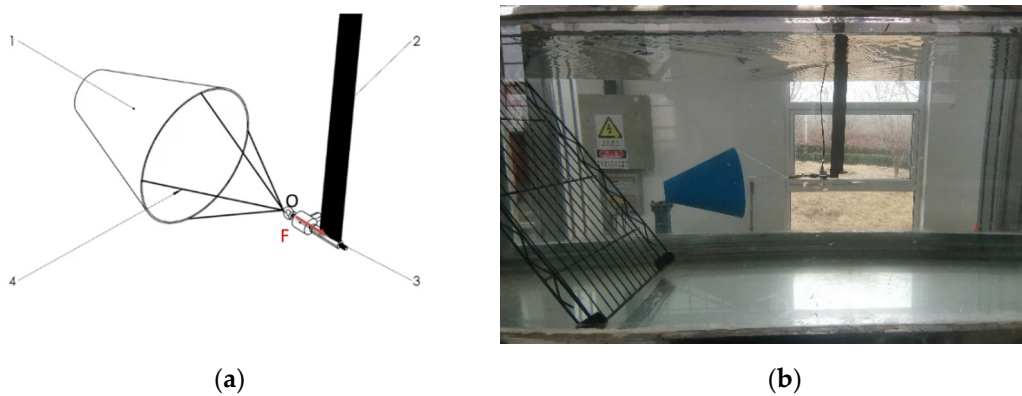


**Figure 5.** Measurement of axial drag forces in experiment, (a) Schematic figure of hydrodynamic loads measurement, 1: cone-shaped drogue; 2: airfoiled plate; 3: DYMH-106D screw tension sensor; 4: nylon lines; (b) Experimental figure of hydrodynamic loads measurement.

The drag force  $F$  on node  $O$  is measured, as illustrated in Figure 5a. The drag force results in strain, which turn to a change in capacitance. Thus, the force signal was converted into an electrical signal for display. The sensor structure is illustrated in Figure 6a. The sensor used in this experiment had a range of 50 N and an accuracy of 0.3%. That is, the confidence interval of the actual force  $F$  is the measured data  $F' \pm 0.15$  N. At the same time, the data were transferred to DAY-SENSOR acquisition software for recording, as shown in Figure 6b. After the cone-shaped drogue was stable in the water, the DAY-SENSOR software started to collect experimental data. Then, the motor of the circulating water tank was powered, and the frequency of the inverter was adjusted to generate a stable flow field with a specific flow rate. The flow rate was maintained for approximately one minute to ensure that the flow field entered a stable state.



**Figure 6.** Data acquisition devices in detail, (a) DYMH-106D tension sensor; (b) Interface of DAY-SENSOR software.

After the data collection time met the requirements, the frequency of the inverter was adjusted to change the flow rate, and the axial force of the cone-shaped drogue was measured at other flow rates.

### 3.3. Experiment Results

According to the actual performance of the water tank and tension sensor, this experiment was mainly carried out at flow rates of 0 m/s, 0.19 m/s, 0.33 m/s, 0.47 m/s, 0.60 m/s, and 0.72 m/s. The force data of the cone-shaped drogue are shown in Figure 7.

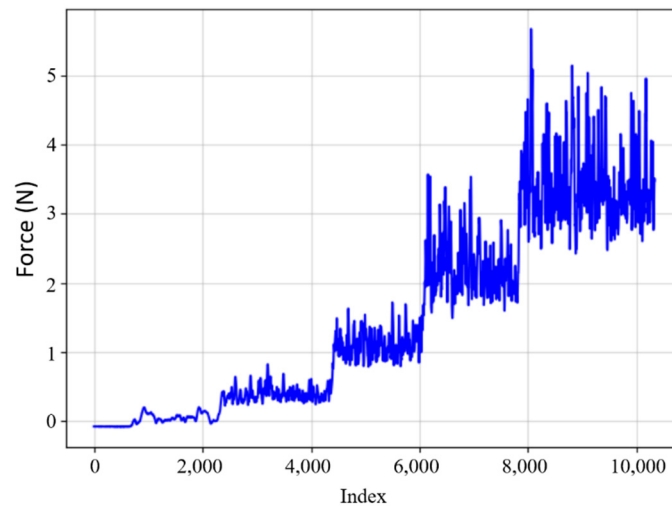


Figure 7. Axial drag forces of drogue in experimental test.

## 4. Virtual Simulation

The virtual simulations were implemented by a co-simulation of RecurDyn and Particleworks. The relative velocity between the drogue and surrounding water was established by flowing water in the experiments, while it was established by moving drogue in the virtual simulations. Motion of the cone-shaped drogue was defined in RecurDyn, and Particleworks performed flow field simulation analysis. The cone-shaped drogue, dummy body, water tank, and kinematic pairs were modelled in RecurDyn, as shown in Figure 8a. The model generated by RecurDyn was imported into the Particleworks software in .obj format, and important parameters such as fluid properties, particle diameter, and integration step were set in Particleworks. After the particles were filled, a solution file was generated, which could be opened in RecurDyn for simulation analysis. The velocity contour of fluid during simulation is shown in Figure 8b.

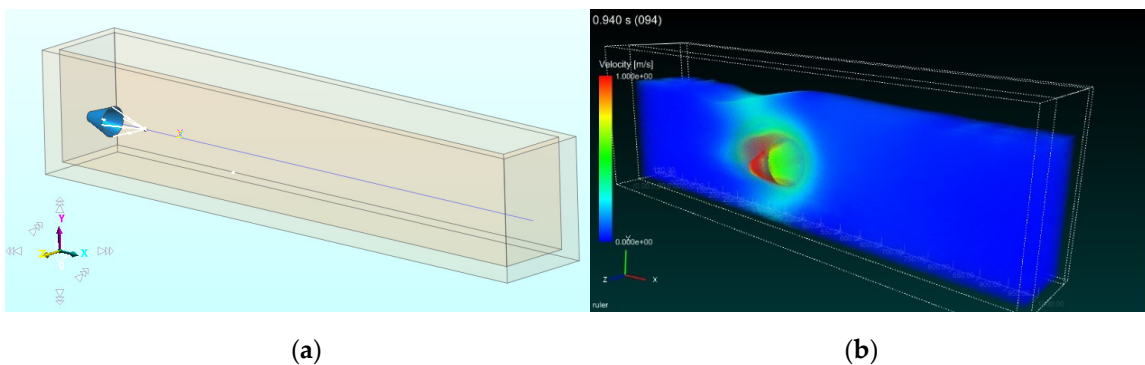


Figure 8. Modelling of towing drogue by co-simulation of RecurDyn and Particleworks. (a) RecurDyn modelling; (b) Particleworks modelling.

#### 4.1. Parameter Tuning

Particleworks is commercial software developed based on the Moving Particle Semi-implicit (MPS) method [26]. The MPS method is an analytical method dealing with incompressible flow, which discretises continuum mechanics using particles. The fundamental governing equations of the MPS method are a continuum equation and Navier–Stokes equations.

Continuum equation (mass conservation law)

$$\frac{D\rho}{Dt} = 0. \tag{4}$$

Navier–Stokes equations (momentum conservation law)

$$\frac{D\vec{u}}{Dt} = -\frac{\nabla P}{\rho} + \nu \nabla^2 \vec{u} + \vec{g}. \tag{5}$$

where  $D/Dt$  expresses a Lagrangian derivation,  $\rho$  is density,  $\vec{u}$  is velocity,  $P$  is pressure,  $\nu$  is kinematic viscosity coefficient, and  $\vec{g}$  is gravity acceleration.

The distance over which an interaction has an effect is designated as the “effective radius” and particles within the effective radius of a specified particle are termed neighbour particles, as shown in Figure 9. To ensure distribution uniformity and isotropy in the placement of neighbour particles, an appropriate value for the effective radius is 3.1 times the length of the initial particle diameter.

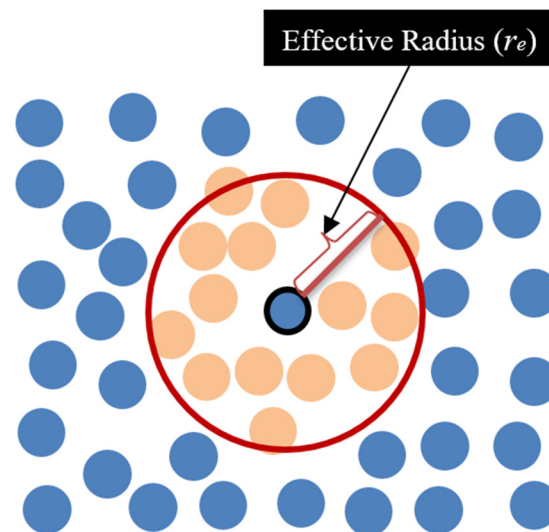


Figure 9. Effective radius of Moving Particle Semi-implicit method.

The interaction between the particles is weighted in accordance with the distance between two particles. The weight function is shown in Equation (6).

$$\omega(|\vec{r}_{ij}|) = \begin{cases} \frac{r_e}{|\vec{r}_{ij}|} - 1 & (|\vec{r}_{ij}| < r_e) \\ 0 & (|\vec{r}_{ij}| \geq r_e) \end{cases}. \tag{6}$$

Subscripts  $i$  and  $j$  express particle numbers.  $r_e$  is the effective radius. In addition,  $\vec{r}_{ij} = \vec{r}_j - \vec{r}_i$ , where  $\vec{r}_i$  is the position vector of particle  $i$ .

Particle number density is a dimensionless quantity expressing the density of particle placement and is a parameter unique to the MPS method. The particle number density is defined by

$$n = \sum_{j \neq i} \omega \left( \left| \vec{r}_{ij} \right| \right). \tag{7}$$

As mentioned above, both the particle size and the integration step greatly affect the simulation results. Since the volume of fluid to be modelled is determined, the number of particles increases exponentially with the decrease of the particle size. The computation cost is inversely proportional to the number of particles. However, the simulation results are unreliable if the particle size is too large. Therefore, calibrating the simulation model through experimental data and selecting the appropriate particle size are necessary prerequisites for the simulation. A cone-shaped drogue of the same size as the one used in physical experiment was established in RecurDyn. In Particleworks, particles with diameters of 6, 5, 4, 3, and 2.6 mm were successively generated for simulation analysis, with integration step sizes of  $1.0 \times 10^{-4}$ ,  $1.5 \times 10^{-4}$ ,  $2.0 \times 10^{-4}$ , and  $3.0 \times 10^{-4}$  s. The results are shown in Figure 10. Within the error tolerance range, the simulation results are stable and fit the physical experiment when the particle diameter was 5 mm and the integration step size was  $1.0 \times 10^{-4}$  s. The difference between the simulation and experimental results is less than 10%.

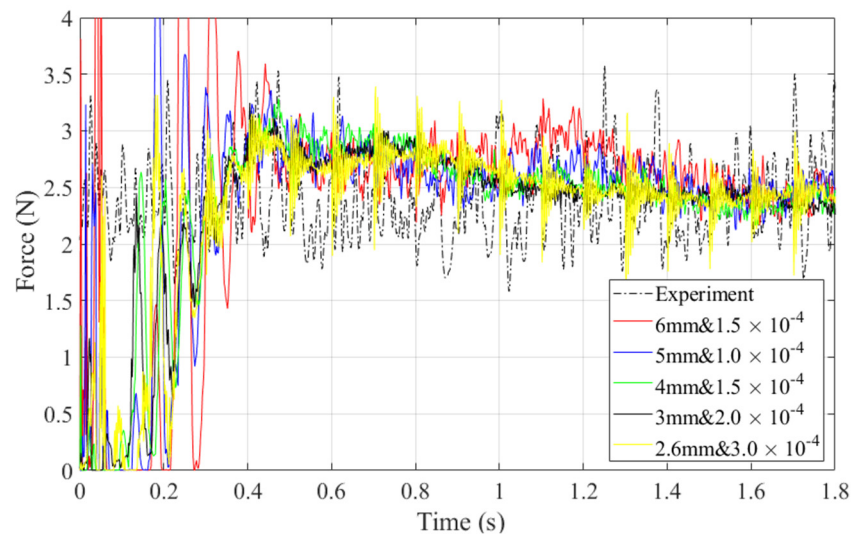


Figure 10. Tuning of particle size and integration step size.

#### 4.2. Building Data Library

After tuning the modelling parameters, simulation analyses were carried out to establish the data library needed for the machine learning. By adjusting the towing speed and rotational angle, nine simulations were carried out, and more than 8500 sets of data were sampled. According to the motion characteristics of the deep-towed multi-channel seismic array system in an actual sea trial [27,28], a reasonable range of design variables was set as following: the range of angles was 0 to 0.533 rad; the range of angular velocity was  $-0.6$  to  $0.52$  rad/s; the angular acceleration was  $-1.29$  to  $2.1$  rad/s<sup>2</sup>; the range of velocity was 0 to 1 m/s; and the acceleration was  $-1.125$  to  $1.5$  m/s<sup>2</sup>. The basic conditions of the rotational angle, angular velocity, angular acceleration, velocity, and acceleration are shown in Table 1. The drag forces  $F_x$  and  $F_y$ , and torque  $M_z$  were obtained. Both the design variables and research objectives of Data 6 are shown in Figure 11. At the beginning of the simulation, the cone-shaped drogue changed from a static state to a stable moving state, and the forces and torque fluctuated significantly. Therefore, part of the data at the beginning of the simulation must be removed. There is a slight fluctuation in the entire

data, which is filtered by low-pass filtering. After transforming coordinates and low-pass filtering, a data library was established. The processed data curve is shown in Figure 12.

**Table 1.** Basic information of design variable in building data library.

	Data1	Data2	Data3	Data4	Data5	Data6	Data7	Data8	Data9
Angle (rad)	0.177	0.262	0.26	0.083	0.015	0.28	0.1	0	0.09
Angular vel. (rad/s)	0.530	0.262	0.26	0.533	0.419	0.52	0.4	0.37	0.52
Angular accel. (rad/s <sup>2</sup> )	0.35	0	0	0.167	0.11	-0.5	-0.6	-0.36	-0.41
	0.35	0	0	0.167	0.3	0.46	0.2	0.52	0.43
Velocity (mm/s)	0	0	0	0	-1.29	-0.93	-2.0	-1.2	-1.02
	0	0	0	0	0.56	0.913	0	2.1	1.46
Acceleration (mm/s <sup>2</sup> )	354.67	194.7	200	99.6	181.2	128.42	137.4	150	14.12
	1062.83	500	650	639.6	500	520	500.3	600	600
Torque (N*mm)	700	0	-300	200	-266.74	-471.2	-322.17	-1125	-750
	700	1071.43	500	200	735.825	471.22	376.971	750	1500

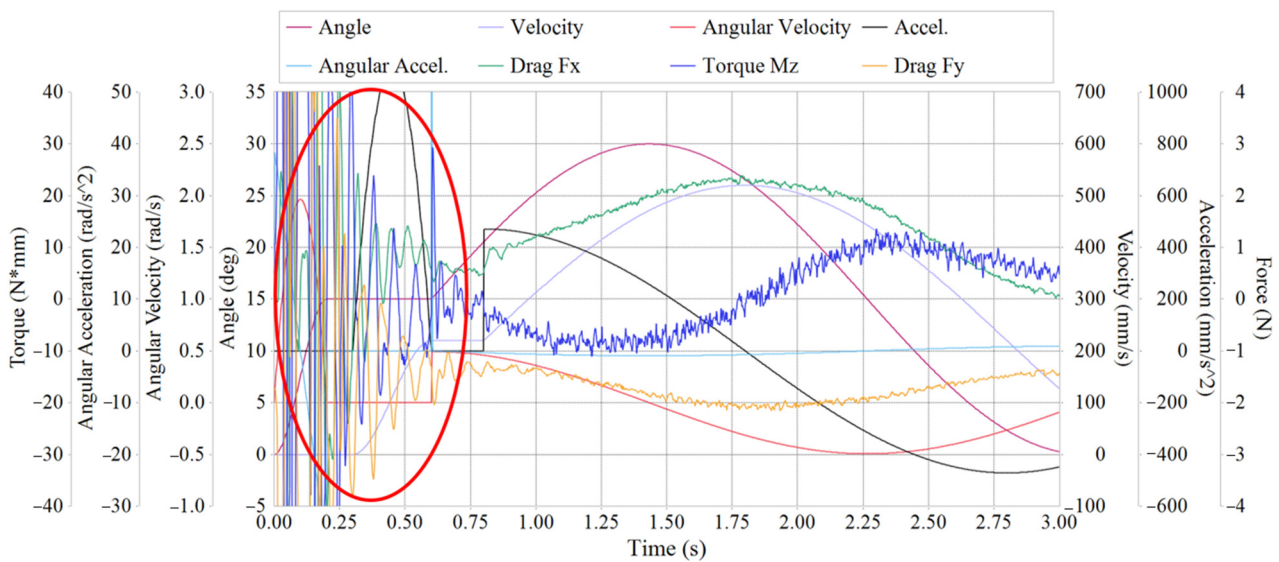


**Figure 11.** Design variables and research objectives of Data 6.

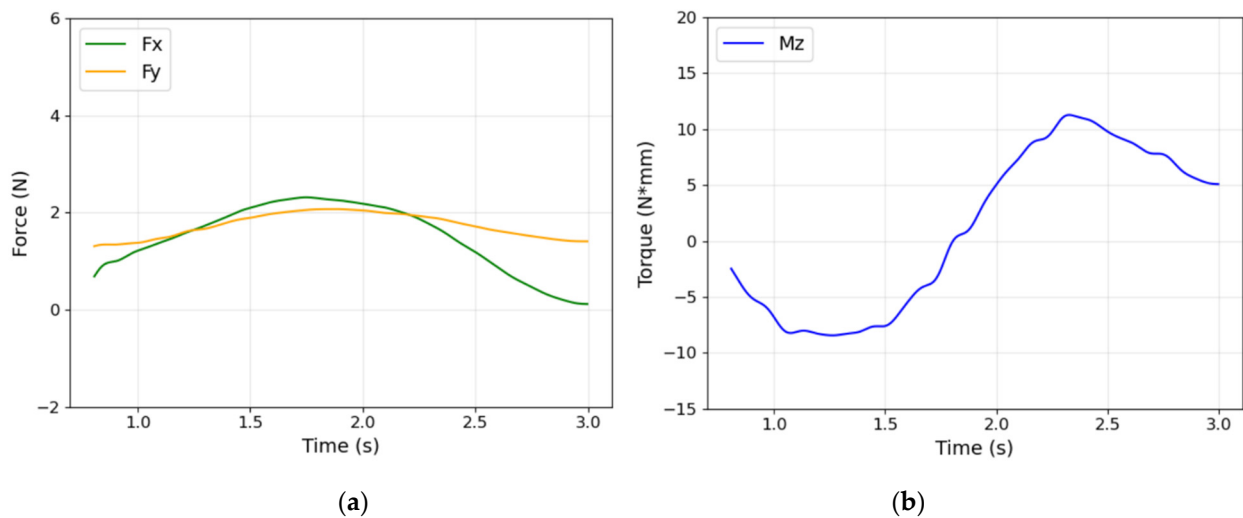


**Figure 12.** Post-processing of simulation results, (a) Post-processing of the drag force, lateral force; (b) Post-processing of the aligning torque.

## 5. Machine Learning Processing

The regression algorithm is mainly used to predict numerical data. In this analysis, it was used to predict the hydrodynamic forces and torque of the cone-shaped drogue. Common regression algorithms include the normal equation, ridge regression, gradient descent in linear regression, polynomial regression algorithm, and neural network regression algorithm. According to the Morison formula, the relationship between the design variables and the research objectives is not a simple linear one. Therefore, polynomial regression and neural network regression algorithm were selected for this study. Both polynomial regression and neural network regression algorithms, called from the Scikit-learn library of the Python tool [29,30], were used to train and predict the relationship between the design variables and the hydrodynamic forces and torque.

### 5.1. Polynomial Regression

The nonlinear relation can be predicted by the polynomial regression method by adding high-order items. The specific formula is given by Equations (8) and (9).

Specific formula of the unary m-degree polynomial regression equation:

$$y = b_0 + b_1x + b_2x^2 + \dots + b_mx^m. \tag{8}$$

Specific formula of the binary quadratic polynomial regression equation:

$$y = b_0 + b_1x_1 + b_2x_2 + b_3x_1x_2 + b_4x_1^2 + b_5x_2^2. \tag{9}$$

where  $b_i$  is the undetermined coefficient.

According to the specific formula of the binary quadratic polynomial regression equation, imagine creating a new set of features, as shown in Equation (10). So, the equation can be written as Equation (11). By considering linear fits within a higher-dimensional space built with these basis functions, the model has the flexibility to fit a much broader range of data.

$$z = [x_1, x_2, x_1x_2, x_1^2, x_2^2]. \tag{10}$$

$$y = b_0 + b_1z_1 + b_2z_2 + b_3z_3 + b_4z_4 + b_5z_5. \tag{11}$$

In this study, there were five design variables, so five-element n-degree polynomials were selected for fitting. We only needed to determine the value of degree n to confirm the final fitting situation. Numerical fitting of the case was related to the value of degree, as shown in Figure 13. The predicted hydrodynamic forces and torque values were compared with their values, and the mean square error (MSE) was used to evaluate the accuracy of the surrogate model. Select the degree where MSE is the smallest, and the specific formula of MSE is shown in Equation (12):

$$MSE = \frac{1}{m} \sum_{i=1}^m (f_i - y_i)^2. \tag{12}$$

where  $f_i$  denotes the predicted value, and  $y_i$  denotes the real value.

After the final test, the polynomial regression could better predict the forces when its degree was 4 and could better predict the torque when the degree was 5. The results will be shown in detail in Section 5.2.3.

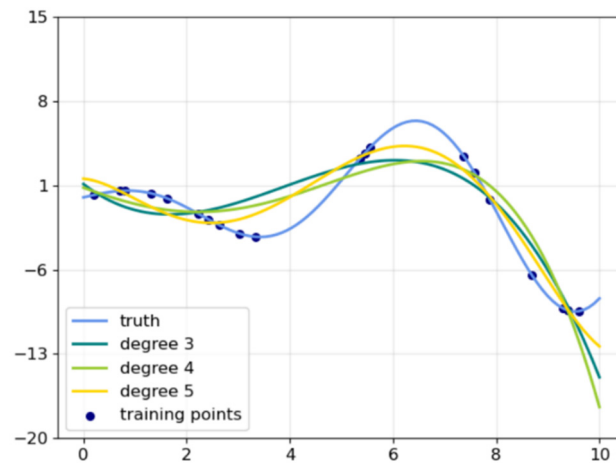


Figure 13. Comparison of fitting conditions of different degrees.

### 5.2. Neural Network Regression

#### 5.2.1. Basic Structure of Neural Networks

A neural network is a multilayer feedforward network. The important processing unit of the network is the topological structure of neurons and networks, which connects a neuron to another layer or another neuron of the same layer. The connection is accompanied by the weight  $\omega$ , which is adjusted by the backpropagation learning algorithm. The process of establishing the learning model involves determining all the parameters in the neural network using the gradient descent method. The number of input and output nodes of the neural network depends on the research problem. The number of input nodes means the number of design variables, and the number of output nodes means the number of research objectives. There are five design variables and three research objectives in the data library, and three neural network models were established to predict the relationship between each research objective and all the design variables. Each neural network model has five input nodes and one output node, as shown in Figure 14.

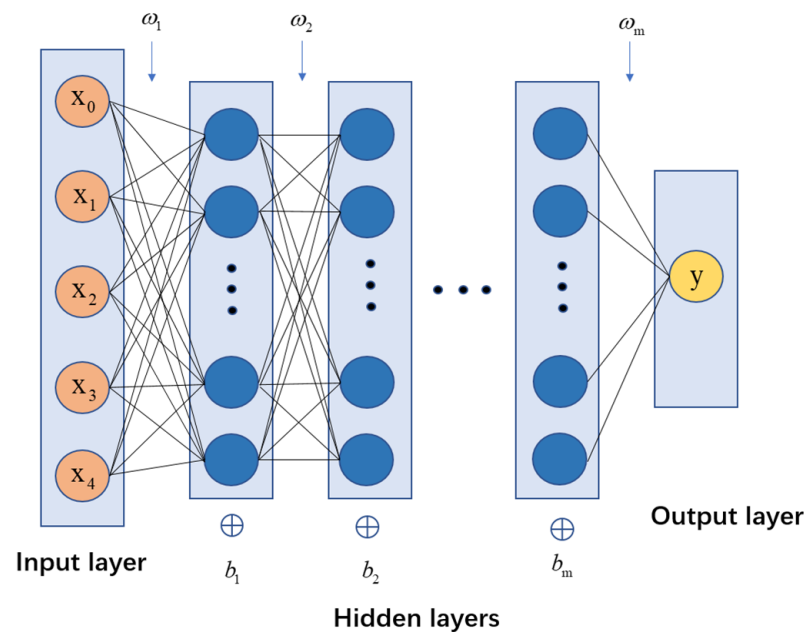


Figure 14. Topology of neural network.

The activation function  $f(\cdot)$  is used to introduce nonlinearity into the neural network, which narrows the value to a smaller range [21], as shown in Figure 15. For example, the sigmoid activation function has a compression range of zero to one, as shown in Equation (13).

There are many activation functions available, of which the ReLU and TanH functions are superior to the sigmoid activation functions, as shown in Equations (14) and (15). In this study, we chose the TanH functions as the activation function.

$$sigmoid(x) = \frac{1}{1 + e^{-x}} \tag{13}$$

$$ReLU(x) = \begin{cases} x, & x \geq 0 \\ 0, & x < 0 \end{cases} \tag{14}$$

$$TanH = 2sigmoid(2x) - 1 = \frac{2}{1 + e^{-2x}} - 1 \tag{15}$$

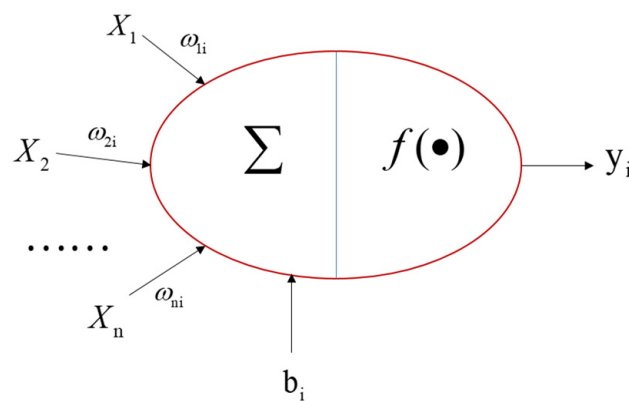


Figure 15. Schematic diagram of neural network.

$X_j$  ( $j = 1, 2, 3, \dots, n$ ) is the input signal accepted by neurons,  $\omega_{ji}$  represents the weight of the  $j$ th neuron in layer  $i$ , and  $b_i$  is the bias. After receiving inputs from neurons of each layer, the weighted sum of all inputs and weights is calculated and the amount of bias is added and then acted on by the activation function as the output of this layer. The input–output relationship is shown in Equation (16).

$$y = f(\omega \cdot x + b) = f\left(\sum_{j=1}^n \omega_{ji} X_j + b\right) \tag{16}$$

### 5.2.2. Establishment of Neural Networks

The number of hidden layers and nodes in each layer have important effects on the training difficulty and prediction performance of the neural network. In general, the more complex the neural network, the more difficult the training and the better the prediction performance. At the same time, however, the risk of overfitting is increased. Regarding the former, some studies [31–34] have shown that the neural network of a single hidden layer can approach any nonlinear function under the condition of a sufficient number of nodes in the hidden layer.

However, there is still no clear quantitative formula for the selection of hidden layer nodes. A rough estimation can be made according to the empirical formula [35,36]:

$$N = \sqrt{n + m} + a \tag{17}$$

where  $N$  is the number of neurons in the hidden layer,  $n$  and  $m$  are the number of input nodes and output nodes,  $a$  is a constant, usually with a value range between 1 and 10.

After preliminary debugging and considering the complexity of the problem in this study, the neural network model of a single hidden layer was used to predict the force, and the number of neurons in the hidden layer was set between 13 and 30. A neural network model with two hidden layers was used to predict the torque. The number of

neurons in the first hidden layer was set between 155 and 165. The number of neurons in the second hidden layer was set between 105 and 115 neurons. When the network layers were determined, the grid search method was used to determine the number of neurons in each layer of the network. In terms of the data, 60% of the data were randomly divided as the training set, 20% as the validation set, and 20% as the testing set. The training set data were used to fit the model. In the neural network, the validation set was used to select the number of neurons in the hidden layer according to the scope of grid search. The testing set was used to evaluate the generalisation capability of the final model. That is, the training set was used to find the rule, and the validation set was used to find the network structure with the best score and take it as the final network structure.

The score was measured by R-squared; the closer R-Squared is to 1, the higher the accuracy of the surrogate model is. The specific formula of R-squared is shown in Equation (18):

$$R^2 = 1 - \frac{\sum_{i=1}^m (f_i - y_i)^2}{\sum_{i=1}^m (y_i - \bar{y}_i)^2} \tag{18}$$

where  $f_i$  denotes the predicted value,  $y_i$  denotes the real value, and  $\bar{y}_i$  denotes the average of the real values.

After validation-set adjustment, the number of nodes in a single hidden layer used to predict the neural network model of  $F_x$  was 27, and  $F_y$  was 27. For the neural network used to predict  $M_z$ , the number of neurons in the first hidden layer was 168, and the number of neurons in the second layer was 110.

### 5.2.3. Results and Discussion

The surrogate model that indicates the relationship between the design variables and the research objectives was generated by the training and validation sets, and five design variables of the testing set were input into the surrogate model to predicate the drag force  $F_x$ , lateral force  $F_y$  and torque  $M_z$ . MSE and R-squared were used to evaluate the accuracy of the surrogate model. The testing data were randomly selected each time, the MSEs of  $F_x$ ,  $F_y$  and  $M_z$  are shown in Table 2, and the R-squared of  $F_x$ ,  $F_y$  and  $M_z$  are shown in Table 3. Meanwhile, the maximum, minimum, and the average values of the  $F_x$ ,  $F_y$ , and  $M_z$  in the obtained data library are listed in Table 4. Compared to the values shown in Table 4, the MSE and the R-squared of predictions by the surrogate model are acceptable.

**Table 2.** MSE of predictions by surrogate model.

	$F_x(N^2)$	$F_y(N^2)$	$M_z(N^2 \cdot mm^2)$
Polynomial Regression	0.0452	0.0015	0.8310
Neural Network Regression	0.0297	0.0019	0.7341

**Table 3.** R-squared of predictions by surrogate model.

	$F_x(N^2)$	$F_y(N^2)$	$M_z(N^2 \cdot mm^2)$
Polynomial Regression	0.9891	0.9929	0.9868
Neural Network Regression	0.9928	0.9910	0.9883

**Table 4.** Basic information of Fx, Fy and Mz in data library.

	Fx (N)	Fy (N)	Mz (N·mm)
Average	2.1722	1.7746	5.4190
MIN	0.0296	0.0020	0.7526
MAX	12.7854	4.8293	23.6963

The drag Fx of the testing set were predicted by both the polynomial and neural network regressions, respectively, and these predicted values were compared with the real values, as shown in Figure 16. Similarly, the Fy and Mz are illustrated in Figures 17 and 18. Several values predicted by the polynomial regression were much larger than the real values, as indicated by green boxes. Except for these values, either the Fx or Fy can be well-predicted by the polynomial regression when its degree is 4, while the aligning torque Mz can be well predicted when the degree is 5. The neural network regression algorithm is more reliable in obtaining the Fx, Fy and Mz, and the maximum MSE is less than 0.8 (N<sup>2</sup>/N<sup>2</sup>·mm<sup>2</sup>) and its R-squared is close to 1. Finally, the surrogate model that maps the relationship between the hydrodynamic characteristics of the cone-shaped drogue and towing conditions was established by using the neural network regression.

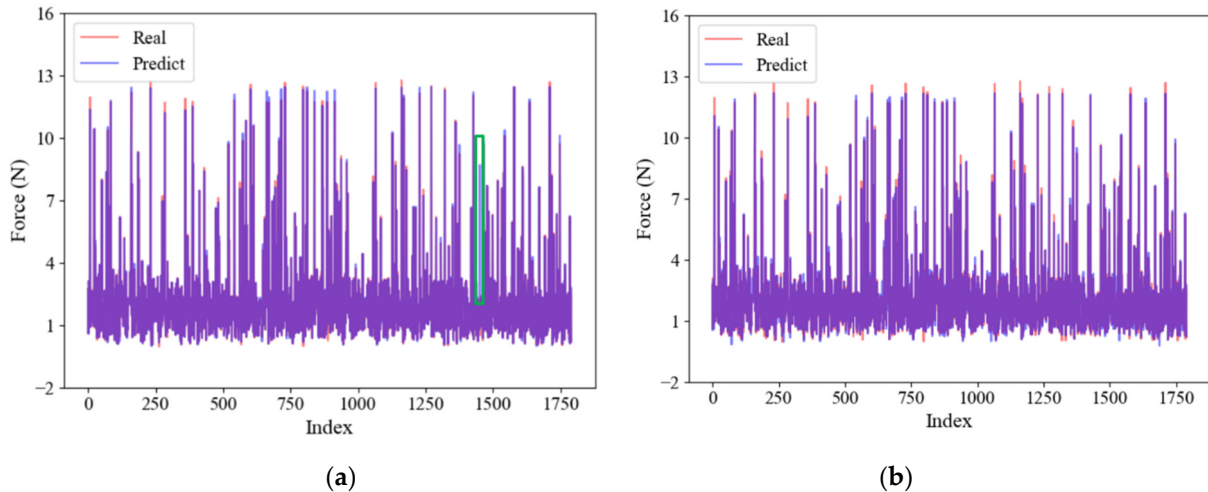


**Figure 16.** Fitting results of Fx by polynomial regression and neural network regression, (a) Polynomial regression; (b) Neural network regression.

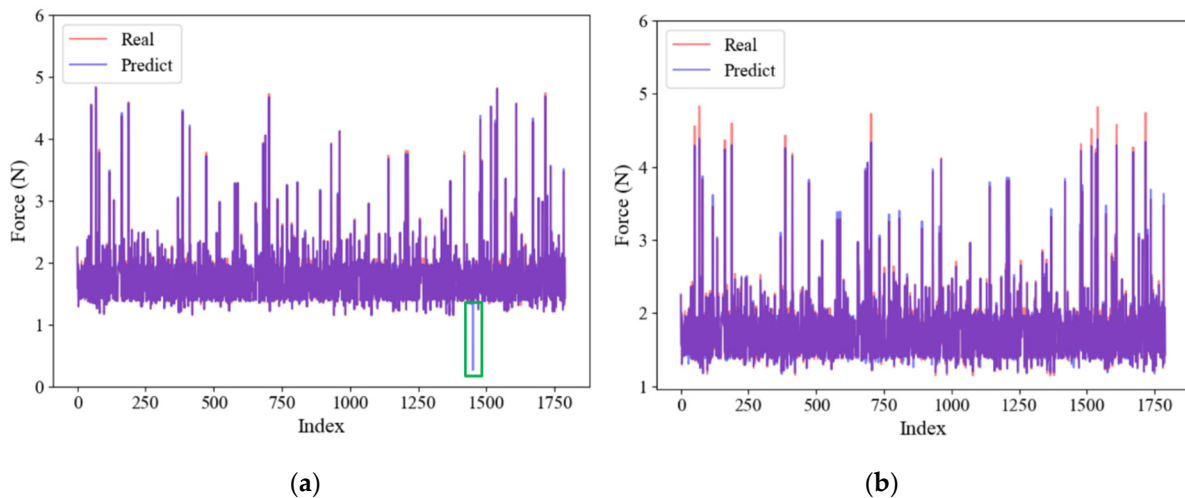


**Figure 17.** Fitting results of Fy by polynomial regression and neural network regression, (a) Polynomial regression; (b) Neural network regression.

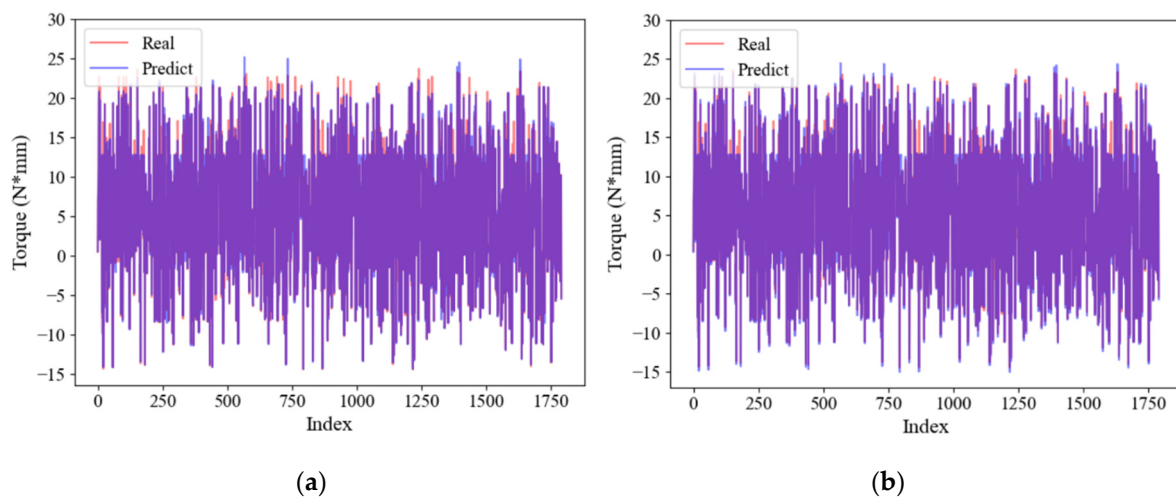


**Figure 18.** Fitting results of  $M_z$  by polynomial regression and neural network regression, (a) Polynomial regression; (b) Neural network regression.

## 6. Summary

Based on data-driven simulations, the surrogate model that maps the relationship between the hydrodynamic characteristics of the cone-shaped drogue and towing conditions was obtained in this paper, so that the effect of a cone-shaped drogue can be embedded into the numerical modelling of the deep-towed seismic survey system. The research results can be summarised as follows:

- (1) The five design variables and three research objectives were determined according to the Morison formula. The rotational angle, angular velocity, angular acceleration, velocity, and acceleration were selected as input design variables, and the drag forces  $F_x$ , lateral forces  $F_y$ , and torque  $M_z$  were respectively taken as the output research objectives. According to the motion characteristics of the towed vehicle and the cone-shaped drogue in actual sea trial, a reasonable range of design variables was set.
- (2) The simulation model was calibrated with the aid of physical experiments to ensure that the simulation results accurately reflected the mapping relationship between the design variables and the research objectives, and a large number of samples were obtained by the simulation model. After transforming coordinates and low-pass filtering of the data, a data library was established.
- (3) Polynomial regression and neural network regression algorithms were used to create the surrogate model. Analysis results show that the surrogate model obtained by machine learning have good performance in predicting research objectives. The results also reveal that the neural network regression algorithm is superior to polynomial regression algorithm and its largest error of mean square is less than  $0.8 (N^2/N^2 \cdot mm^2)$  and its R-squared is close to 1. Therefore, the surrogate model that maps the relationship between the hydrodynamic characteristics of the drogue and towing conditions was established successfully.

Considering the applicability of the surrogate model, we plan to continue the following work in the future:

- (1) As the information of the current step is merely adopted to predict the research target, neither the polynomial regression nor neural network regression considers the cumulative effect of the front steps. Therefore, the current surrogate model is fit for situations in which the cumulative effect of the front steps is not obvious, such as the exploration stage of the deep-towed system. In the future, the time-series algorithm will be used to model the diving and rising stages, during which the cumulative effect is non-negligible.

- (2) The geometry of the cone-shaped drogue is unchanged here. The geometry of the cone-shaped drogue will be set as an independent variable so that the cone-shaped drogue can be optimised to stabilise the deep-towed system.

**Author Contributions:** Conceptualization, X.Z.; methodology, X.Z. and M.S.; software, M.S. and J.-H.C.; validation, T.H., L.Z. and X.Z.; formal analysis, M.S. and T.H.; investigation, X.Z.; resources, Kai-ben Yu; data curation, M.S. and T.H.; writing—original draft preparation, M.S.; writing—review and editing, X.Z. and J.-H.C.; visualization, M.S.; supervision, X.Z.; project administration, X.Z.; funding acquisition, X.Z., L.Z. and K.Y. All authors have read and agreed to the published version of the manuscript.

**Funding:** This research was funded by National Natural Science Foundation of China (Grant No.51909145), and the National Key R&D Program of China (Grant No. 2016YFC0303901).

**Institutional Review Board Statement:** Not applicable.

**Informed Consent Statement:** Not applicable.

**Data Availability Statement:** The data presented in this study are available on request from the corresponding author.

**Acknowledgments:** This work was supported by Key Laboratory of High-efficiency and Clean Mechanical Manufacture at Shandong University, Ministry of Education; National Demonstration Center for Experimental Mechanical Engineering Education at Shandong University; Young Scholars of Shandong University and Rizhao Intelligent Manufacturing Institute; and the Fundamental Research Funds of Shandong University. The authors would like to acknowledge FunctionBay Inc. and Prometech Software Inc. for providing license files of RecurDyn and Particleworks, respectively.

**Conflicts of Interest:** The authors declare no conflict of interest.

## References

- Chapman, N.R.; Gettrust, J.F.; Walia, R.; Hannay, D.; Spence, G.D.; Wood, W.T.; Hyndman, R.D. High-resolution, deep-towed, multichannel seismic survey of deep-sea gas hydrates off western Canada. *Geophysics* **2002**, *67*, 1038–1047. [[CrossRef](#)]
- Pei, Y. Analysis of the Motion and Study on the Constant-Depth Control of the Deep Sea. Master's Thesis, Shanghai Jiao Tong University, Shanghai, China, 2011.
- Sengupta, A.; Machin, R.; Bourland, G.; Longmire, E.; Bissell, D. Performance of a conical ribbon drogue parachute in the wake of a subscale Orion command module. In Proceedings of the IEEE Aerospace Conference, Big Sky, MT, USA, 3–10 March 2012.
- Kitamura, K.; Fukumoto, K.; Mori, K. Numerical Study of Surface Pressure Fluctuation on Rigid Disk-Gap-Band-Type Supersonic Parachutes. *AIAA J.* **2020**, *58*, 5347–5360. [[CrossRef](#)]
- Williams, A.N. Wave Forces on Inclined Circular Cylinder. *J. Waterw. Port Coast. Ocean. Eng.* **1985**, *111*, 910–920. [[CrossRef](#)]
- Liu, S.G. Comments on the hydrodynamics research of offshore structure. *Adv. Mech.* **1986**, *3*.
- Lokenath, D.; Matiur, R. A theory of nonlinear wave loading on offshore structures. *Int. J. Math. Math. Sci.* **1981**, *4*, 589–613.
- Shu, C.W. High-order finite difference and finite volume WENO schemes and discontinuous galerkin methods for CFD. *Int. J. Comput. Fluid Dyn.* **2003**, *17*, 107–118. [[CrossRef](#)]
- Wang, J.; Xiao, H. Data-Driven CFD Modeling of Turbulent Flows Through Complex Structures. *Int. J. Heat Fluid Flow* **2016**, *62*, 138–149. [[CrossRef](#)]
- Duan, G.T.; Koshizuka, S.; Yamaji, A.; Chen, B.; Li, X.; Tamai, T. An accurate and stable multiphase moving particle semi-implicit method based on a corrective matrix for all particle interaction models. *Int. J. Numer. Methods Eng.* **2018**, *115*, 1287–1314. [[CrossRef](#)]
- Koshizuka, S.; Shibata, K.; Kondo, M.; Matsunaga, T. *Moving Particle Semi-Implicit Method: A Meshfree Particle Method for Fluid Dynamics*; Academic Press: Cambridge, MA, USA, 2018.
- Matsunaga, T.; Sodersten, A.; Shibata, K.; Koshizuka, S. Improved treatment of wall boundary conditions for a particle method with consistent spatial discretization. *Comput. Methods Appl. Mech. Eng.* **2020**, *358*, 112624. [[CrossRef](#)]
- Deng, X.; Wang, S.; Hammi, Y.; Qian, L.; Liu, Y. A combined experimental and computational study of lubrication mechanism of high precision reducer adopting a worm gear drive with complicated space surface contact. *Tribol. Int.* **2020**, *146*, 106261. [[CrossRef](#)]
- Khayyer, A.; Tsuruta, N.; Shimizu, Y.; Gotoh, H. Multi-resolution MPS for incompressible fluid-elastic structure interactions in ocean engineering. *Appl. Ocean Res.* **2019**, *82*, 397–414. [[CrossRef](#)]
- Spandonidis, C.C.; Spyrou, K.J. Coupled vessel-dry-granular-cargo roll dynamics in regular beam seas. *Ocean Eng.* **2016**, *120*, 238–245. [[CrossRef](#)]

16. Wang, Y.; Zhao, W.; Liang, L.; Wu, Q.; Jin, H.; Wang, C. A Review on Optimal Design of Fluid Machine Learning Method. *Chin. J. Turbomach.* **2020**, *62*, 77–90.
17. Parish, E.J.; Duraisamy, K. A paradigm for data-driven predictive modeling using field inversion and machine learning. *J. Comput. Phys.* **2016**, *305*, 758–774. [[CrossRef](#)]
18. Singh, A.P.; Medida, S.; Duraisamy, K. Machine-Learning-Augmented Predictive Modeling of Turbulent Separated Flows over Airfoils. *AIAA J.* **2017**, *55*, 2215–2227. [[CrossRef](#)]
19. Milano, M.; Koumoutsakos, P. Neural network modeling for near wall turbulent flow. *J. Comput. Phys.* **2002**, *182*, 1–26. [[CrossRef](#)]
20. Fukami, K.; Fukagata, K.; Taira, K. Super-resolution reconstruction of turbulent flows with machine learning. *J. Fluid Mech.* **2019**, *870*, 106–120. [[CrossRef](#)]
21. Lin, H.; Wang, Y. A bp neural network method of confirming the morison equation's hydrodynamic coefficients. *China Offshore Platf.* **2005**, *20*, 6.
22. Bonakdar, L.; Etemad-Shahidi, A. Predicting wave run-up on rubble-mound structures using M5 model tree. *Ocean Eng.* **2011**, *38*, 111–118. [[CrossRef](#)]
23. Bonakdar, L.; Oumeraci, H.; Etemad-Shahidi, A. Wave load formulae for prediction of wave-induced forces on a slender pile within pile groups. *Coast. Eng.* **2015**, *102*, 49–68. [[CrossRef](#)]
24. Srinivasan, P.A.; Guastoni, L.; Azizpour, H.; Schlatter, P.; Vinuesa, R. Predictions of turbulent shear flows using deep neural networks. *Phys. Rev. Fluids* **2019**, *4*, 054603. [[CrossRef](#)]
25. Theodoropoulos, P.; Spandonidis, C.C.; Themelis, N.; Giordamalis, C.; Fassois, S. Evaluation of Different Deep-Learning Models for the Prediction of a Ship's Propulsion Power. *J. Mar. Sci. Eng.* **2021**, *9*, 116. [[CrossRef](#)]
26. SolutionGroup. *Particleworks Theory Manual Release 7.0.0*; Prometech Software Inc.: Tokyo, Japan, 2020.
27. Zhu, X.Q.; Wang, Y.F.; Yoo, W.S.; Nicoll, R.; Ren, H. Stability analysis of spar platform with four mooring cables in consideration of cable dynamics. *Ocean Eng.* **2021**, *236*, 109522. [[CrossRef](#)]
28. Zhu, X.; Wei, Z.; Pei, Y.; Yu, K.; Le, Z. Dynamic modeling and position prediction of deep-towed seismic array. *J. Shandong Univ. (Eng. Sci.)* **2020**, *50*, 9–16.
29. Abraham, A.; Pedregosa, F.; Eickenberg, M.; Gervais, P.; Mueller, A.; Kossaifi, J.; Gramfort, A.; Thirion, B.; Varoquaux, G. Machine learning for neuroimaging with scikit-learn. *Front. Neuroinformatics* **2014**, *8*, 14. [[CrossRef](#)]
30. Pedregosa, F.; Varoquaux, G.; Gramfort, A.; Michel, V.; Thirion, B.; Grisel, O.; Blondel, M.; Prettenhofer, P.; Weiss, R.; Dubourg, V.; et al. Scikit-learn: Machine Learning in Python. *J. Mach. Learn. Res.* **2011**, *12*, 2825–2830.
31. Bolcskei, H.; Grohs, P.; Kutyniok, G.; Petersen, P. Optimal Approximation with Sparsely Connected Deep Neural Networks. *Siam J. Math. Data Sci.* **2019**, *1*, 8–45. [[CrossRef](#)]
32. Brunton, S.L.; Noack, B.R.; Koumoutsakos, P. Machine Learning for Fluid Mechanics. *Annu. Rev. Fluid Mech.* **2020**, *52*, 477–508. [[CrossRef](#)]
33. Hornik, K.; Stinchcombe, M.; White, H. Multilayer feedforward networks are universal approximators. *Neural Netw.* **1989**, *2*, 359–366. [[CrossRef](#)]
34. Li, X.; Liu, G. The improvement of BP algorithm and its application. *J. Sichuan Univ. (Eng. Sci. Ed.)* **2000**, *32*, 105–109.
35. Shen, H.; Wang, Z.; Gao, C.; Qin, J.; Yao, F.; Xu, W. Determining the number of BP neural network hidden layer units. *J. Tianjin Univ. Technol.* **2008**, *2008*, 13–15.
36. Feisi Technology Product Research and Development Center. *Neural Network Theory and MATLAB7 Implementation*; Electronic Industry Press: Beijing, China, 2005.